

Performance comparison of the MODIS and the VIIRS 1.38 μm cirrus cloud channels using libRadtran and CALIOP data

Lang Xia^{a,b,e}, Fen Zhao^d, Liping Chen^{a,e}, Ruirui Zhang^{a,e}, Kebiao Mao^{b,c,*}, Arve Kylling^f, Ying Ma^b

^a Beijing Research Center of Intelligent Equipment for Agriculture, Beijing Academy of Agriculture and Forestry Sciences, Beijing 100081, China

^b National Hulunber Grassland Ecosystem Observation and Research Station, Institute of Agricultural Resources and Regional Planning, Chinese Academy of Agricultural Sciences, Beijing 100081, China

^c State Key Laboratory of Remote Sensing Science, Institute of Remote Sensing and Digital Earth Research, Chinese Academy of Science and Beijing Normal University, Beijing, China

^d Key Laboratory of Ecosystem Network Observation and Modeling, Institute of Geographic Sciences and Natural Resources Research, University of Chinese Academy of Science, Beijing 100086, China

^e Beijing Key Laboratory of Intelligent Equipment for Agriculture, Beijing Academy of Agriculture and Forestry Sciences, Beijing 100081, China

^f Norwegian Institute for Air Research, P.O. Box 100, 2027, Kjeller, Norway

ARTICLE INFO

Keywords:

VIIRS M9
MODIS band 26
Cirrus cloud
Performance

ABSTRACT

The top-of-the-atmosphere (TOA) reflectances of the Visible Infrared Imaging Radiometer (VIIRS) M9 channel and the Moderate Resolution Imaging Spectroradiometer (MODIS) 26 channel have been simulated using the libRadtran radiative transfer model and the Cloud-Aerosol Lidar with Orthogonal Polarization (CALIOP) Vertical Feature Mask data. The simulated data were analyzed to quantify the performance differences between the VIIRS M9 and the MODIS 26 channels. Analysis of simulated clear-sky TOA reflectances showed that compared MODIS channel 26, the VIIRS M9 channel always performs better in reducing background reflectance regardless of latitude, season, surface type, vapor content or surface elevation. For mid-latitude, sub-Arctic and tropical regions the VIIRS M9 channel reduce the background reflectance by approximately 66.7%, 52.6% and 41.5%, respectively over the surface type of sandstone, compared to MODIS channel 26. Simulations for cloudy skies showed that both stratus and cumulus clouds contribute less to VIIRS M9 and MODIS band 26 TOA reflectances. Analysis of observed MODIS, VIIRS and CALIOP data was consistent with the simulated results. The VIIRS M9 decreases clear-sky background reflectance by as much as 35.96% and non-cirrus cloud reflectance by 29.86% compared with the MODIS channel 26. The observed reflectances of MODIS and VIIRS cirrus channels for clear-sky, non-cirrus cloud, and cirrus cloud are 0.0133 and 0.0095, 0.020 and 0.015, 0.084 and 0.067 respectively.

1. Introduction

Satellite remote sensing is the most efficient method for observing global cirrus cloud activities. Among the current satellite cirrus detection methods, 1.38 μm cirrus test method is the most effective daytime cirrus cloud detection algorithm (Xia et al., 2015). The 1.38 μm water vapor absorbing band was first used to obtain cirrus cloud information from the Airborne Visible/Infrared Imaging Spectrometer (AVIRIS) data (Gao et al., 1993) in 1993. Then, the Moderate Resolution Imaging Spectroradiometer (MODIS) (Justice et al., 1998) was launched on the Terra satellite in 1998 is a satellite sensor with a 1.38 μm cirrus cloud detection channel that greatly improves cirrus cloud detection in daytime. Because of rapid global climatic changes, research has since focused on global energy radiation balances, as terrestrial global change

requires increasingly accurate cirrus cloud data (Sun et al., 2011; Kazantzidis et al., 2011; Roy et al., 2014). As a result, many new sensors have been designed to incorporate the 1.38 μm cirrus cloud channels to monitor cirrus cloud activities. These sensors include the Suomi National Polar-orbiting Partnership (Suomi NPP) Visible Infrared Imaging Radiometer (VIIRS) (Cao et al., 2013; Xia et al., 2014), the Landsat 8 Operational Land Imager (OLI) (Barsi et al., 2014), and the Sentinel-2 multi-spectral instrument (MSI) (Drusch et al., 2012) et al.

Since 1.38 μm channel plays important role in the cirrus cloud community, e.g. cirrus cloud characteristics, thin cirrus path radiances correction etc., many studies have utilized it. For example, Gao and Kaufman (1995) used the MODIS 1.375- μm channel to correct thin cirrus contamination in 0.4 to 1.0 μm region. Yang et al. (2001) studied cirrus bidirectional reflectance by using the MODIS 1.38 μm cirrus data.

* Corresponding author at: National Hulunber Grassland Ecosystem Observation and Research Station, Institute of Agricultural Resources and Regional Planning, Chinese Academy of Agricultural Sciences, Beijing 100081, China.

E-mail address: maokebiao@caas.cn (K. Mao).

<https://doi.org/10.1016/j.rse.2017.12.040>

Received 17 February 2017; Received in revised form 7 October 2017; Accepted 27 December 2017
0034-4257/ © 2017 Elsevier Inc. All rights reserved.

Table 1
Characteristics of the VIIRS M9 and the MODIS band 26 channels and CALIOP.

Sensor band	Swath width (km)	Band (nm)	Bandwidth (nm)	Resolution (m)	Quantization (bit)	SNR Require/on orbit
MODIS 26	2330	1360–1390	30	1000	12	229/150
VIIRS M9	3000	1371–1386	15	750	12	227/83
CALIOP	0.333	532/1064		not fixed	14	83/50

Note: Lidars do not have a swath width and resolutions of the CALIOP change with altitudes.

Xu (2002) researched scattering characteristics of small ice circular cylinders in 1.38 μm data. Gao et al. (2002) presented a method to differentiate dust from cirrus clouds using the 1.38 μm /1.24 μm reflectance ratio. Another study area has focused on cirrus cloud parameter retrievals and energy radiation balances. For example, Gao et al. (1993) used the 1.38 μm band to detect cirrus clouds in 1993 for AVIRIS data. The MODIS Cloud Mask Algorithm (Ackerman et al., 1999; Frey et al., 2008) performs the 1.38 μm test only when the elevation is above 2000 m or when the total precipitable water over land surfaces falls below 0.75 cm to avoid false alarms. Roskovensky and Liou (2003) combined the 1.38 μm /0.65 μm reflectance ratio with 8.6–11 μm brightness temperature differences to enhance thin cirrus cloud detection. The VIIRS Cloud Mask algorithm used the total precipitable water as the function to obtain the cirrus detection thresholds (Hutchison et al., 2012) to overcome vapor content shortages. Xia et al. (2015) added an 11 μm brightness temperature and a multiday average land surface temperature test to improve MODIS and VIIRS cirrus detection performance in the Tibet region. Kovalsky and Roy (2015) analyzed conterminous United States cirrus and non-cirrus clouds by using the Landsat 8 cirrus band.

Although many studies have been conducted regarding the 1.38 μm cirrus cloud channel, no research analyzes the actual performance differences between the newly designed VIIRS 1.38 μm and the MODIS 1.38 μm channels under different situations. In addition, current cirrus test methods (Frey et al., 2008; Hutchison et al., 2014; Baker, 2014; Xia et al., 2015) for the 1.38 μm channel focus only on one or two influence factors, e.g., vapor content or land type. None of the methods analyze how the 1.38 μm channel performs under different geolocations, altitudes, atmospheric parameters, cloud types, land types, or viewing angles for MODIS and VIIRS, and these factors are important for designing a reasonable cirrus test method and obtaining more precise thresholds. Hence, this study compared and analyzed simulated data from the libRadtran radiative transfer model and observed data from the Cloud-Aerosol Lidar with Orthogonal Polarization (CALIOP) in detail for the VIIRS and the MODIS cirrus channels to identify how the improved and newly designed VIIRS cirrus channel performs better than the MODIS cirrus channel. The comparison and analysis data will be a reference to develop more precise cirrus-cloud detection methods.

2. Background

2.1. Radiative transfer in the 1.38 μm channel

The main application of the 1.38 μm channel is cirrus cloud detection. Hence, the radiative transfer simulations must carefully include the relevant cloud optical properties. Many studies considered the radiative transfer of the cloudy sky, and especially the cirrus cloud (or ice) radiative transfer characteristics (Liou, 1973; Hu and Stamnes, 1993; Fu, 1996; Liou, 2002; Key et al., 2002; Yang et al., 2013; Baum et al., 2014). A simplified, but illustrative, description of the radiative transfer in the 1.38 μm channel was given by the Eq. (1) (Liou, 2002) which illustrates how the VIIRS M9 and MODIS 26 channels are affected by cirrus clouds and other factors.

$$I = I_g + I_c \quad (1)$$

Here, I is the radiance obtained by the sensor, I_g represents the two-way radiation (solar to ground, ground to sensor), I_c is the radiation reflected by the cirrus cloud that arrives at the sensor. The relative magnitudes of I_g and I_c will change as the cloud optical thickness changes. For instance, when the cloud is optically relatively thick and the surface reflected radiance cannot penetrate the cirrus cloud, $I_g = 0$, and I is mainly influenced by the cirrus cloud altitude which determines the water vapor content between the cirrus cloud top and sensor, and solar zenith angle, viewing angle etc. When the cirrus cloud is optically thin, radiation reflected of the surface may pass through the cirrus cloud. Thus I_g will be different from zero and I will be influenced by surface type and altitude, and the water content in the total atmosphere.

2.2. Dataset and libRadtran

MODIS is the key instrument aboard the Terra and Aqua satellites. It acquires global data in 36 spectral bands within every 1 to 2 days. Due to high temporal resolution, high quality data products, easy access and other features, MODIS is widely used by researchers to track changes in the Earth system (Justice et al., 2002). VIIRS extends from MODIS and the Advanced Very High Resolution Radiometer (AVHRR) which has a viewing swath width greater than 2330 km and can provide global observation information within 1 to 2 days. CALIOP, carried by the Cloud-Aerosol Lidar and Infrared Pathfinder Satellite, was launched in 2006 and provides specific information about cloud and aerosol profiles that is often used to evaluate the accuracy of cloud and aerosol retrieval algorithms (Holz et al., 2008; Chan and Comiso, 2011; Hiraoka et al., 2014; Xia et al., 2015). Table 1 shows some characteristics of the VIIRS and the MODIS cirrus channels and CALIOP.

The MODIS level 1B granular data, the VIIRS level 1 5-min swath SDR and GEO 750 m data downloaded from Goddard Space Flight Center (GSFC), were used in this study. The MODIS band 26 and the VIIRS M9 reflectance were obtained from the L1 B data with low-quality pixels removed using Uncertainty Index (dataset EV_Band26_Uncert_Indexes for MODIS and QF1_VIIRSMBANDSDR_M9 for VIIRS) (Toller et al., 2003). The profile information data used in comparison was the CALIOP Level 2 5-km Vertical Feature Mask (VFM, Product version 3.30) data, which describes the vertical and horizontal distribution of cloud and aerosol profiles (each profile was divided into 545 layers with fixed vertical and horizontal resolutions for each layer) observed by the CALIOP (Hunt et al., 2009).

To simulate the VIIRS M9 and the MODIS 26 channel radiances at TOA, the libRadtran software package version 2.0.1 was used (www.libradtran.org) (Mayer and Kylling, 2005; Emde et al., 2016). The libRadtran was adopted as simulation software in this study because it can support a lot of alternative parameterizations of ice crystal habit directly (Fu, 1996; Yang et al., 2013; Baum et al., 2014), which is important to analyze the feature of cirrus cloud. The radiative transfer equation was solved using the improved discrete-ordinate (DISORT) method by Buras et al. (2011), which is based on the versatile and much used DISORT algorithm by Stamnes et al. (1988). The spectral resolution was 0.1 nm and gaseous absorption included using the parameterization by Gasteiger et al. (2014). Various surface characteristics, clouds and ambient atmospheres were included as specified in the

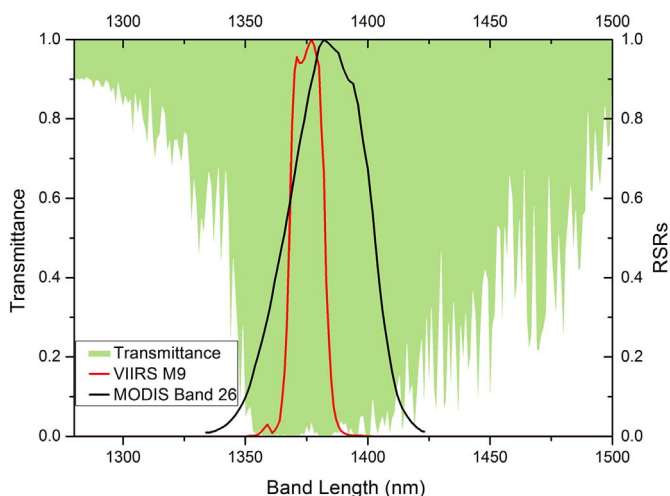


Fig. 1. Atmospheric transmittance corresponding to spectrum response regions of the VIIRS M9 and the MODIS band 26 (at water vapor content of 1.0 g/cm²).

sections below.

2.3. Difference between the VIIRS and the MODIS cirrus channels

The pre-launch and on-orbit calibrations showed that the Terra and Aqua MODIS shortwave and mid-wave infrared bands (bands 5, 6, 7, 26) suffered from a thermal leak problem, primarily caused by an optical leak at the mid-wave infrared band, and an electronic crosstalk problem (Xiong et al., 2004). These problems caused a sizable out-of-band response effect to the MODIS 1.38 μm channel. When designing VIIRS sensor, the engineers added a blocking filter to a focal plane, and the VIIRS 1.38 μm channel is no longer affected by the out-of-band response effect. Besides, in order to increase the sensitivity to cirrus clouds, the VIIRS M9 was designed with a bandwidth of 15 nm, whereas the bandwidth of the MODIS band 26 is 30 nm, as shown in Fig. 1. Also, the VIIRS M9 channel has a better signal-to-noise ratio (SNR) than the MODIS band 26 (Uprety et al., 2013; Xiong et al., 2014).

In theory, the improved design makes the VIIRS M9 channel more sensitive to water vapor absorption than MODIS channel 26, since the M9 channel has a narrower band width and a better out-of-band response, see Fig. 1. On the other hand, the different center wavelengths of the VIIRS M9 and MODIS 26 channels might cause different performance for the same atmospheric and surface conditions due to the wavelength dependence of the reflectance, absorption and scattering characteristics. Also, the better SNR for the VIIRS M9 channel implies that there might be improved detection of optically thin cirrus clouds compared to the MODIS channel 26, that is the VIIRS M9 is more sensitive than MODIS band 26 to cirrus clouds. Hence, the following sections analyze in detail how the narrower bandwidth and the filter design improve cirrus cloud detection capabilities.

Table 2
The simulation parameters used in Sections 3.1, 3.2, and 3.3.

Number	Simulation parameters						
	Vapor (g/cm ²)	Land type	Elevation (km)	Solar zenith angle (degree)	Viewing zenith angle (degree)	Cloud	Solar azimuth angle (degree)
Fig. 2	*	Sandstone	0.0	17	0	no	−110
Fig. 3	0.5, 2.0	*	0.0	17	0	no	−110
Fig. 4	2.0	Sandstone	*	17	0	no	−110
Fig. 5	0.5, 2.0	Sandstone	0.0	*	*	no	−110
Fig. 6	2.0	Sandstone	0.0	17	0	*	−110

3. Comparison of the libRadtran simulations

For a strong 1.38 μm vapor absorption band, e.g. the VIIRS M9 and the MODIS band 26, band-mean absorption efficiency factor is a concise indicator to evaluate performance. Specifically, the band-mean absorption efficiency factor refers to the ratio of the absorption cross section and the geometric cross section of the particle projected onto a plane perpendicular to the incident direction (Wendisch and Yang, 2012). As shown in Fig. 1, the VIIRS M9 presents larger band-mean absorption efficiency factor than the MODIS band 26. However, the purpose of designing the 1.38 μm channel is mainly for cirrus cloud detection, and the current cirrus cloud detection algorithm of 1.38 μm channel for MODIS and VIIRS usually takes the TOA reflectance as input data directly. Hence, in order to make the result of this study directly applicable to design a more accurate test method for cirrus cloud detection, we used TOA reflectance instead of the band-mean absorption efficiency factor in this study.

The main simulation parameters used in Sections 3.1 to 3.3 are listed in Table 2. Since the solar azimuth angle contributes less than the other parameters, the solar azimuth angle was not discussed as an important variable and set to a fixed value in the simulation analyses. Besides, a common solar zenith angle with 17 degree and solar azimuth angle with −110 degree were used in the simulation. In Table 2, * means that the parameter is not a constant and will be analyzed with the simulations.

Eq. (2) was used to indicate performance difference between VIIRS M9 and MODIS band 26 in the analyses.

$$P = \frac{\rho_{26} - \rho_{m9}}{\rho_{26}} \times 100\%, \tag{2}$$

where P indicates the variation percentage of TOA reflectance simulated by the VIIRS M9 relative to the MODIS band 26, ρ_{26} represents the TOA reflectance of the MODIS band 26, and ρ_{m9} represents the TOA reflectance of the VIIRS M9. An alternative interpretation of Eq. (2) is that it shows the reduction percentage of the reflectance as measured by VIIRS M9 compared to MODIS channel 26.

3.1. Vapor, land type and surface elevation

The principle of the 1.38 μm cirrus cloud detection is based on vapor absorption in this band (Gao and Kaufman, 1995). With sufficient atmospheric vapor present (approximately 0.4 g/cm²) in the radiation transmission path, the radiation from the earth surface or low-altitude cloud is masked by the vapor content absorption and cannot reach the sensor. When cirrus cloud is present, the reflected radiance from the cirrus cloud is less influenced by the vapor content because the atmosphere between the cirrus clouds and the sensor is usually very dry. Hence, if the TOA reflectance observed by MODIS band 26 in one pixel exceeds a particular value (threshold), then this pixel will be labeled as a cirrus cloud covered pixel. This is the basic logic of the current cirrus cloud test method for the MODIS and the VIIRS 1.38 μm cirrus cloud detection algorithms (Frey et al., 2008; Baker, 2014). Under the same observation situations, if a sensor with the 1.38 μm channel presents

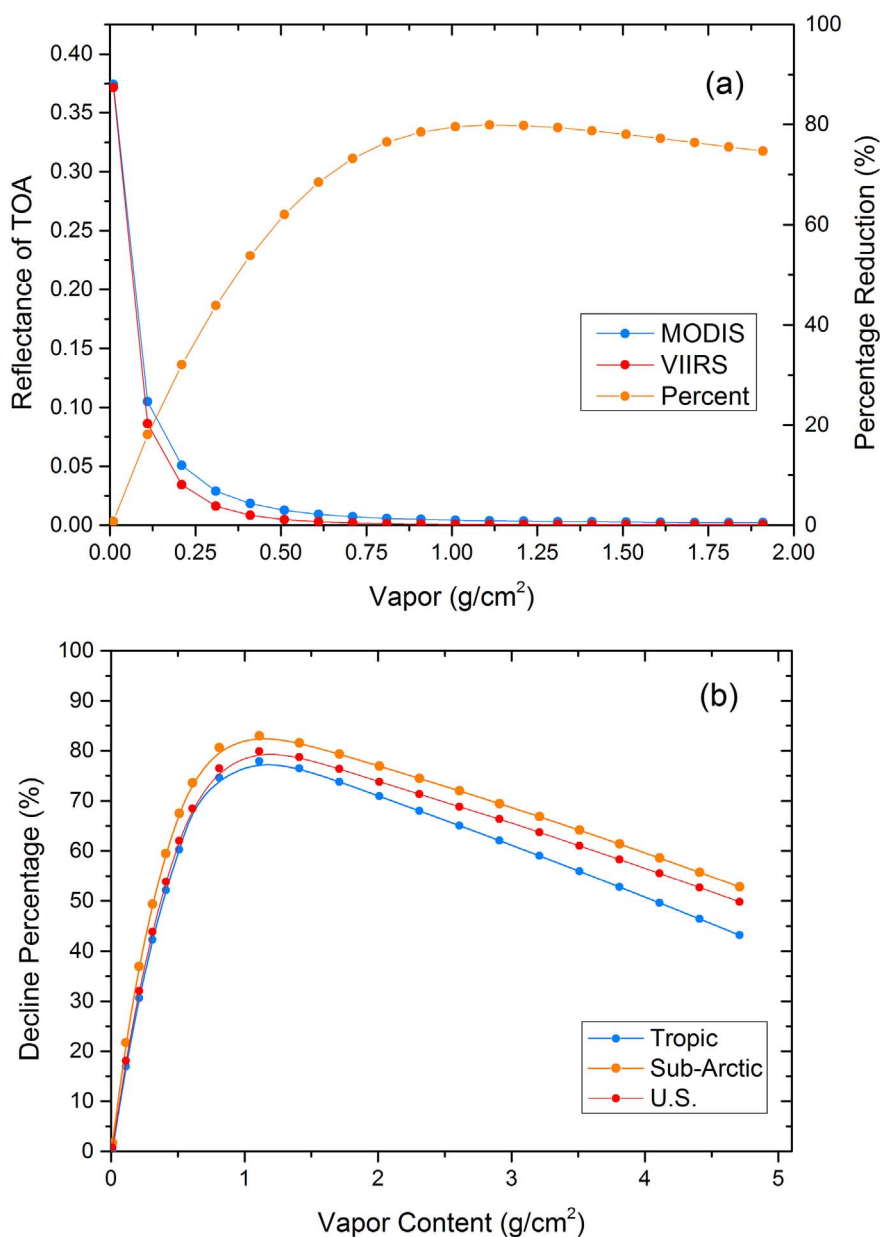


Fig. 2. (a) The clear-sky TOA reflectance of the VIIRS and the MODIS cirrus cloud channels for vapor content between 0.01 and 1.91 g/cm² (when the vapor content is greater than 2.0 g/cm², the reflectances for both VIIRS and MODIS cirrus cloud channels are small, so the part with vapor greater than 2.0 g/cm² is not shown); (b) the reduction percentage of the TOA reflectances between the VIIRS M9 and the MODIS band 26 for different model atmospheres.

smaller TOA reflectance than other sensors for non-cirrus, e.g. clear sky, stratus, we consider this sensor performing better in cirrus cloud detection than others.

In the present study, the variation of water vapor content was simulated firstly. Fig. 2(a) shows the clear-sky reflectance of the MODIS and the VIIRS cirrus cloud channels at different water vapor contents for the U.S. standard model atmosphere (more parameters are listed in Table 2).

As seen in Fig. 2(a), the TOA reflectances for both the VIIRS M9 and the MODIS band 26 decrease as the vapor content increasing, and when water vapor content is less than 0.5 g/cm², the clear-sky TOA reflectance increases dramatically as the water vapor content decreasing, especially when the water vapor content is less than 0.2 g/cm². Generally, for the U.S. model atmosphere, regardless of vapor content changes, the TOA reflectance of the VIIRS M9 is always smaller than the MODIS band 26. This indicates the VIIRS M9 performs better than the MODIS band 26 under the same vapor content. On the other hand, the vapor content decreases as the altitude increasing. Different model atmospheres: tropic, sub-Arctic, and U.S. model atmospheres, with vapor ranges from 0.01 to 4.71 g/cm² were simulated and the detailed

reduction percentage of the TOA reflectance was showed in Fig. 2(b). As shown in Fig. 2(b), the VIIRS M9 presents smaller clear-sky TOA reflectance than the MODIS band 26, and the reflectance is reduced by 74% at most for a water content 1.2 g/cm².

Various surface types with different reflectivity substantially influence the final energy reaching the sensor. The sensitivity to the surface characteristics for the VIIRS M9 and the MODIS band 26 were simulated for the U.S. standard model atmosphere over seven surface types: water, coarse granular snow, conifers grass, deciduous trees, black loam and arkosic sandstone, as shown in Fig. 3(a) and (b). All the spectral information of these materials was obtained from the NASA JPL spectral library (Baldrige et al., 2009).

In Fig. 3(a), when the water vapor is relatively moderate (2.0 g/cm²), the TOA reflectance of the VIIRS M9 is barely affected by the surface backgrounds. However, for the MODIS band 26, the situation was opposite, especially for bright surfaces, e.g., sandstone. As shown in Fig. 3(b), when the vapor drops to 0.5 g/cm², both the VIIRS M9 and the MODIS band 26 are greatly influenced by bright surfaces and less impacted by dark backgrounds, such as water and conifers grass.

The reduction percentages of TOA reflectance calculated by Eq. (2)

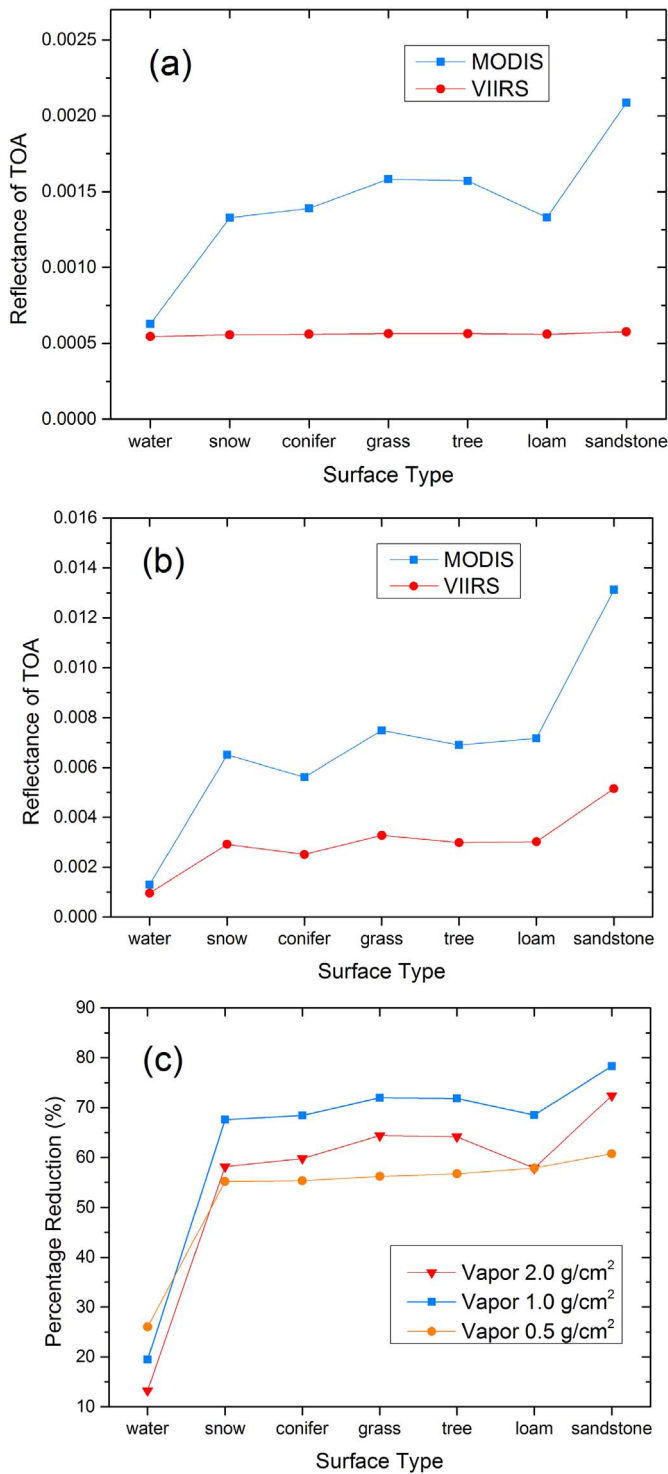


Fig. 3. (a) The clear-sky TOA reflectance results with a vapor content of 2.0 g/cm²; (b) 0.5 g/cm² over seven surface types for the VIIRS M9 and the MODIS band 26; (c) the TOA reflectance reduction percentage between the VIIRS M9 and the MODIS band 26.

between the VIIRS M9 and the MODIS band 26 with vapor contents at 0.5, 1.0 and 2.0 g/cm² are shown in Fig. 3(c). In general, the VIIRS M9 suppresses TOA reflectance caused by different surface types better than the MODIS band 26. The reduction percentage of the maximum TOA reflectance for bright surfaces is approximately 80%, and the reduction percentage of the TOA reflectance is less than 15% for dark ground. The difference in reduction percentages indicated that the VIIRS M9 performs better over bright surfaces than dark surfaces

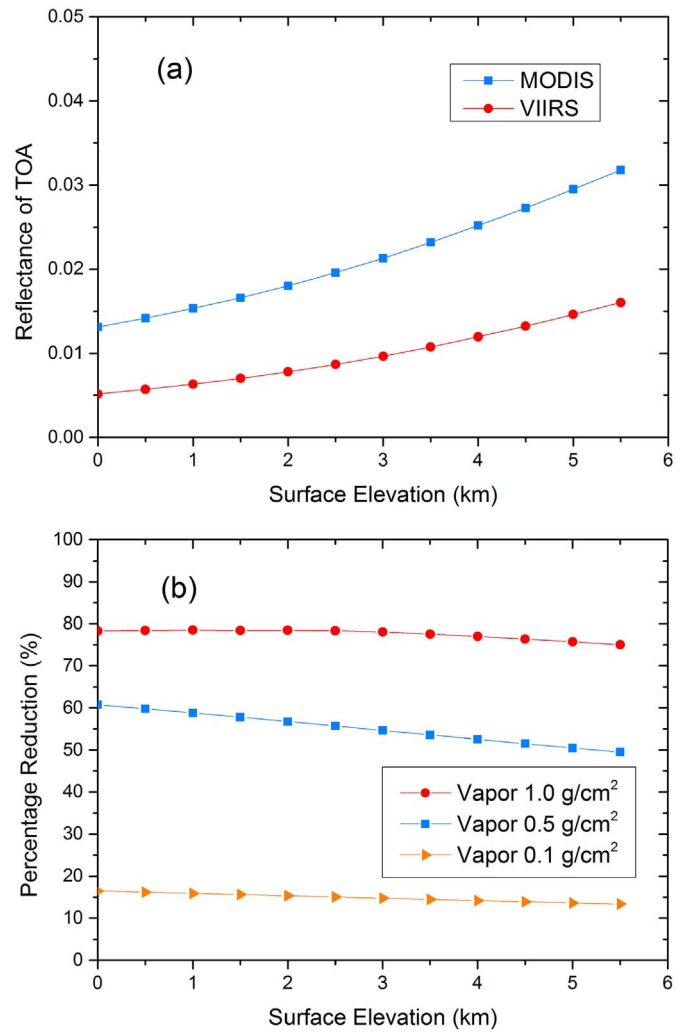


Fig. 4. (a) The clear-sky TOA reflectance of the VIIRS M9 and the MODIS band 26 under different surface elevations; (b) the reduction percentage of the TOA reflectance between VIIRS M9 and the MODIS band 26.

compared with the MODIS band 26, despite the fact that bright surfaces presents greater reflectance than dark backgrounds under the same conditions.

Generally, atmospheric water vapor content drops with increasing surface elevation, and the TOA reflectance increases significantly along with increasing atmospheric transmittance. As a result, the MODIS 1.38 μm cirrus cloud test does not perform when the surface elevation is greater than 2000 m. The clear-sky TOA reflectance of the two channels with surface elevations from 0 m to 5500 m under the U.S. standard model atmosphere is simulated as shown in Fig. 4(a). The result shown in Fig. 4(a) indicates that when the surface elevation increases, the clear-sky TOA reflectance increases, and no matter how the surface elevation changes, the TOA reflectance of the VIIRS cirrus cloud channel is always lower than that of the MODIS.

The reduction percentages of TOA reflectance under vapor content of 0.1, 0.5 and 1.0 g/cm² are shown in Fig. 4(b). According to Fig. 4(b), the performance difference between the VIIRS M9 and the MODIS band 26 varies with the change of surface elevation. VIIRS can reduce approximately 80% more of the background reflectance than the MODIS band 26 when the surface elevation is approximately 0 km, and as the surface elevation increasing, the reflectance reduction percentage decreases. In fact, as the surface elevation reaches 5.5 km (the vapor content is abundant e.g. 2.0 g/cm²), the reflectances for both the MODIS and the VIIRS M9 are greater than 0.01 (as shown in Fig. 4(a))

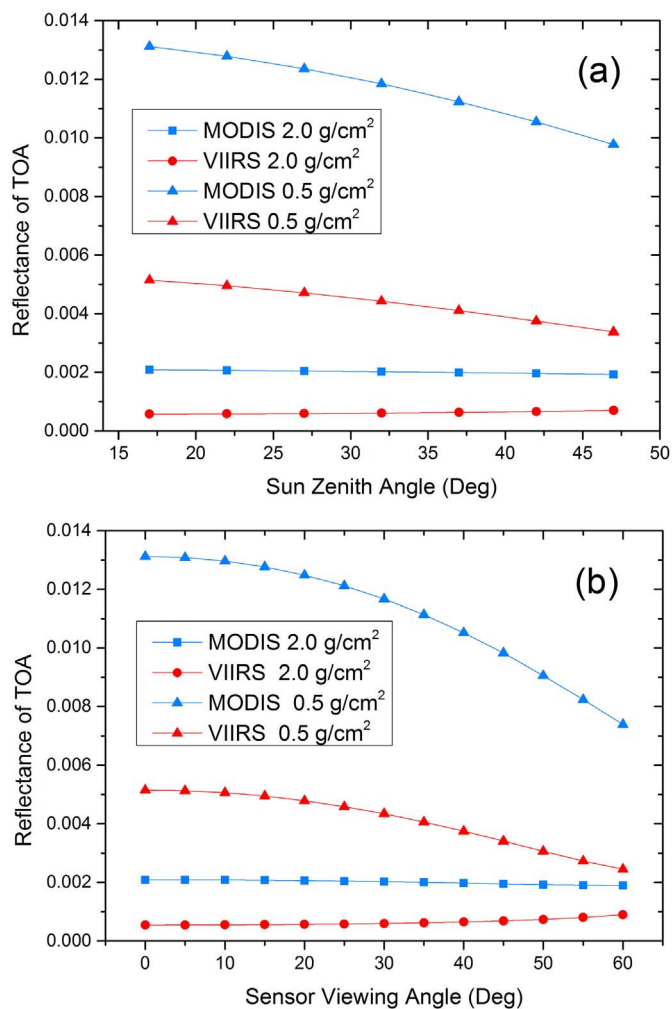


Fig. 5. (a) The clear-sky TOA reflectance of VIIRS and the MODIS cirrus cloud channels for solar zenith angles ranging from 17 to 47 degrees; (b) the clear-sky TOA reflectance of the VIIRS and the MODIS cirrus cloud channels for sensor viewing angles ranging from 0 to 60 degrees.

which is greater than the reflectance for most thin cirrus clouds. This means that it is very difficult to distinguish thin cirrus clouds from the land surface.

3.2. Solar zenith angle and sensor viewing angle

In satellite remote sensing, the solar zenith angle influences the incident radiation, and the viewing zenith angle influences the path length of the radiation transmission between the observed object and the sensor. Changes in both the solar zenith angle and the sensor viewing angle will result in different clear-sky background reflectance. In this section, the clear-sky TOA reflectance was simulated for the MODIS and the VIIRS cirrus cloud channels at different solar zenith angles and sensor viewing angles under a low vapor content of 0.5 g/cm^2 and a moderate vapor content of 2.0 g/cm^2 , as shown in Fig. 5. At higher water vapor levels, such as 2.0 g/cm^2 , variations of the solar zenith angle and the sensor viewing angle have little influence on the TOA reflectance. When the water vapor content is 0.5 g/cm^2 , the low water vapor absorbs less reflected energy from the earth's surface. The variations of the solar zenith angle and the sensor viewing angle contribute more to the TOA reflectance than the vapor content of 2.0 g/cm^2 . Similar to the simulation results for surface types, vapor content and surface elevation, the VIIRS M9 always produces lower TOA reflectance than the MODIS band 26 for all simulated zenith and viewing angles.

3.3. Cirrus and non-cirrus

For the current $1.38 \mu\text{m}$ cirrus cloud test method, the ability to identify cirrus cloud mainly depends on reflectance differences between cirrus cloud and background. The factors affecting the reflectance include not only the factors shown in Sections 3.1 and 3.2 but also non-cirrus clouds, such as cumulus and altostratus, which have been neglected in previous research. In this section, different cloud base altitudes and thicknesses for cirrus, altostratus, stratus and cumulus clouds are analyzed to evaluate the performance of the VIIRS M9 and the MODIS band 26 for the U.S. standard model atmosphere.

Fig. 6 shows the simulated TOA reflectances of stratus, cumulus, altostratus and cirrus cloud under different cloud-base altitudes, effective droplet radii, liquid/ice water contents and cloud thicknesses for the VIIRS M9 and the MODIS band 26. The cloud thickness is defined as the altitude difference between the highest and lowest cloud profile boundary altitude for which either water droplet or ice particle density is positive. The cloud base altitude and thickness were adopted from the MODerate resolution atmospheric TRANsmission (MODTRAN) cloud models (Berk et al., 2005). Cirrus cloud optical properties were calculated using the model provided by Yang et al. (2013). The detailed cloud properties used in the simulation are listed in Table 3.

The special optical properties of cirrus cloud, especially thin cirrus cloud, allow the radiance from the background to pass through the cirrus cloud easily and be detected by the sensor. For the $1.38 \mu\text{m}$ channel, the TOA radiance for cirrus clouds is determined not only by the water vapor content in the radiative transfer path, but also by the cloud altitude and cloud optical properties. In Fig. 6(a), when the cirrus cloud thickness is small, the MODIS band 26 displays greater TOA reflectance than the VIIRS M9. This is due to the background radiance can pass through the cirrus cloud and contributes more to the TOA reflectance than the thin cirrus, as presented in Section 2.1 Eq. (1). However, it does not enhance MODIS's ability to detect cirrus cloud, for the VIIRS M9 eliminates more background reflectance than the MODIS band 26, as shown in Section 3.1 and 3.2. In addition, Fig. 6(a) indicates that when the cirrus cloud thickness or cloud base altitude are small, neither the VIIRS nor the MODIS cirrus cloud bands can detect thin cirrus with a high degree of confidence. For example, when the cirrus cloud thickness is 300 m, the cirrus cloud reflectance is approximately 0.02 (optical thickness about 1.0), which is similar to the reflectance of some surface types or a cumulus cloud with a cloud-base altitude of approximately 3.0 km.

When cirrus cloud has high altitude and large thickness, the background barely contributes to the TOA reflectance. As shown in Fig. 6(b), when the cloud-base altitude is higher than 12 km and cirrus cloud thickness is 1000 m, the TOA reflectance of the VIIRS M9 is slightly larger than the MODIS band 26. This is due to the radiance from the cirrus cloud cannot be attenuated by the vapor when the vapor content between the cirrus cloud top and sensor is extremely low, and cirrus cloud reflectance for VIIRS center band is slightly larger than the center band for the MODIS cirrus cloud channel (Liou, 2002). But one should notice that in a real atmosphere, the vapor content in each layer may not be consistent with the atmospheric profile used in the simulation, and the reflectance performance will be different as shown in the Fig. 6(a).

As the cloud-base altitude decreases, the altostratus reflectance in Fig. 6(c) shows that the VIIRS M9 has lower TOA reflectance than the MODIS band 26. In addition, when the altostratus cloud-base altitude is greater than 5 km, the altostratus cloud provides large TOA reflectance, and thin cirrus clouds with a small extinction coefficient may not be distinguished from the altostratus clouds in the extratropics for the current MODIS and the VIIRS $1.38 \mu\text{m}$ cirrus cloud test methods (Frey et al., 2008; Hutchison et al., 2012).

In general, stratus and cumulus clouds are usually locate at low altitude and contribute little to $1.38 \mu\text{m}$ reflectance. The reflectances for stratus and cumulus clouds are shown in Fig. 6(d) and (e). As it

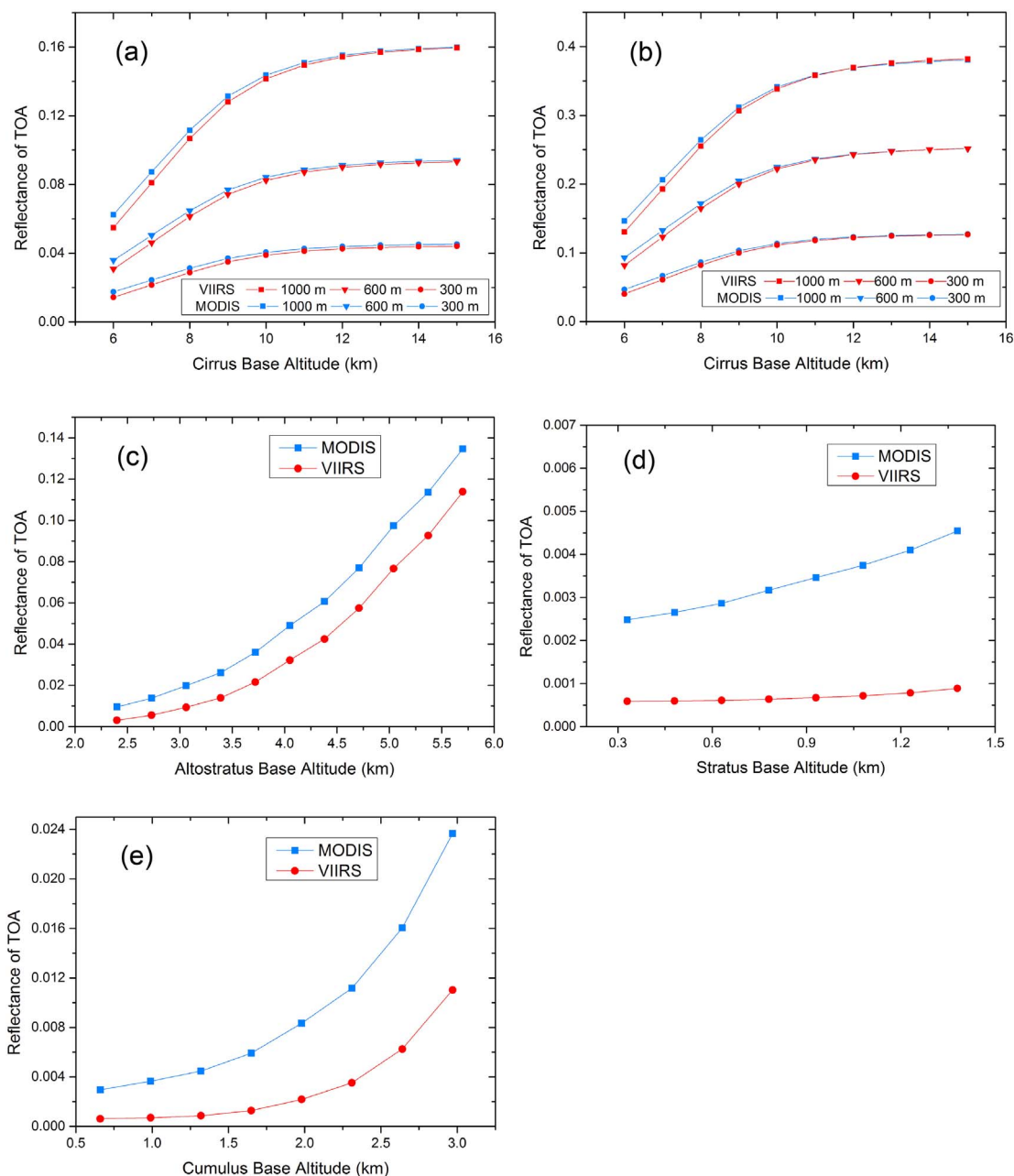


Fig. 6. The TOA reflectance for the VIIRS and the MODIS cirrus cloud channels under different base altitudes and (a) ice water content of 0.03 g/cm³, (b) ice water content of 0.08 g/cm³, (c) altostratus cloud, (d) stratus cloud, and (e) cumulus cloud.

Table 3
Cloud thickness, cloud-base altitude, liquid/ice water content and effective droplet radius used in the simulation.

Cloud type	Thickness (km)	Cloud base altitude (km)	Liquid/ice water content (g/m ³)	Effective droplet radius (μm)
Cirrus	0.3, 0.6, 1.0	6.0 to 15	0.03/0.08	20
Altostratus	0.3	2.4 to 5.7	0.2	8
Stratus	0.34	0.33 to 1.38	0.28	7.3
Cumulus	0.34	0.66 to 2.97	0.26	5.8

shown that when the cloud-base altitude is less than 3 km, the maximum TOA reflectances of stratus cloud in the simulation for the MODIS band 26 and the VIIRS M9 are within 0.005 and 0.001 respectively. These values are very similar to the clear-sky TOA reflectance of most

land types. For cumulus clouds, the maximum TOA reflectance occurs at the cloud-base altitude of 2.97 km with values of 0.024 and 0.01 for the MODIS band 26 and the VIIRS M9.

Fig. 7 shows the detailed variation percentages of the TOA reflectance between the VIIRS M9 and the MODIS band 26 calculated using Eq. (2). As can be seen in Fig. 7, when the cloud-base altitude is less than 5.75 km, the MODIS band 26 has greater TOA reflectance than the VIIRS M9. This indicates that the VIIRS M9 is more effective in suppressing the radiance from non-cirrus clouds than the MODIS band 26. When the cloud-base altitude ranges from 6 km to 11 km, the MODIS band 26 presents slightly larger TOA reflectance than the VIIRS M9 for cirrus clouds with a cloud-base altitude greater than 6 km. However, this situation has no influence on the cirrus cloud detection algorithm because the MODIS band 26 presents a larger TOA reflectance over non-cirrus cloud and clear-sky situations than the VIIRS M9. Besides, as shown in Fig. 7, when the cloud-base altitude is greater

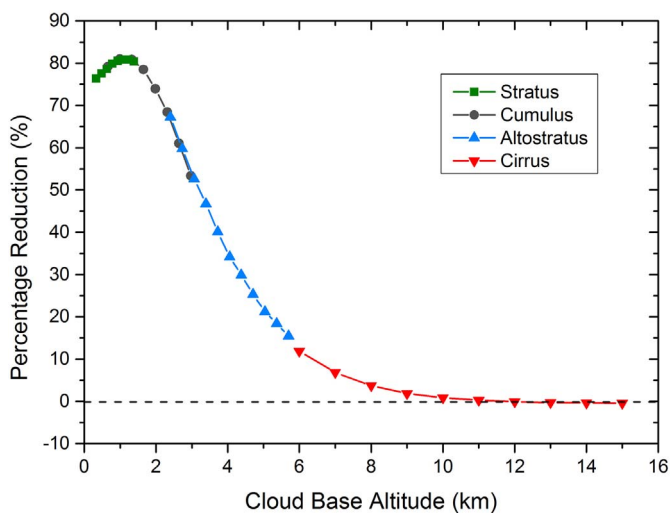


Fig. 7. The variation percentages of the TOA reflectance between the VIIRS M9 and the MODIS band 26 for stratus, cumulus, altostratus, and cirrus clouds with ice water content of 0.08 g/cm^3 and cloud thicknesses of 1000 m.

than 11 km, the VIIRS M9 TOA reflectance is slightly greater than the MODIS band 26 due to the low vapor content between the cirrus cloud and sensor, and the thick optical thickness of the cirrus which obstructs the background radiance.

3.4. Regional and temporal simulations

The influences of the sensor viewing angle and the solar zenith angles, as well as vapor, surface types, surface elevation, and clear-sky reflectance were analyzed in Sections 3.1 and 3.2. In this section, a comparative analysis is presented for different locations (tropical region, sub-polar region and mid-latitude region) with satellite-observed water vapor amounts. In the simulation, the MODIS 8-day synthetic water product in one year was used (Kaufman and Gao, 1992; Hubanks et al., 2015) and the time for each day was set to 1:30 PM as same as the MODIS and VIIRS pass over. It is very difficult to obtain the real reflectance of $1.38 \mu\text{m}$ for the corresponding object in one year for the surface type changing with season, thus a constant surface type (standalone) was used in this study. Another reason to select the surface type as standalone is that the surface type with relative large reflectance will present the maximum difference between the two sensors for different regions. Different model atmospheres are chosen for each season and region. The detailed geographical position of the analyzed regions is shown in Table 4.

Fig. 8 illustrates the simulation results. In general, for each region the reflectance changes in different seasons due to the variation in the vapor content, and the reflectances in winter and spring are larger than other seasons. For mid-latitude region, the VIIRS M9 channel reduces the background reflectance by about 66.7% compared to the MODIS band 26. For sub-polar region, the narrow-band VIIRS cirrus cloud channel performs less efficiently than it does for mid-latitude region that have relatively sufficient water vapor. Overall, the VIIRS M9 channel reduces the background reflectance by approximation 52.6% compared with the MODIS band 26. For tropical regions, due to the high vapor during the entire year, the background contributes less to

Table 4
The geographical positions for the simulation regions used in the study.

Region	Latitude (deg)	Longitude (deg)	Elevation (m)
Mid-latitude	32.0	83.0 W	0.0
Sub-polar	60.0	115.0 E	50.0
Tropical	0.0	113.0 E	50.0

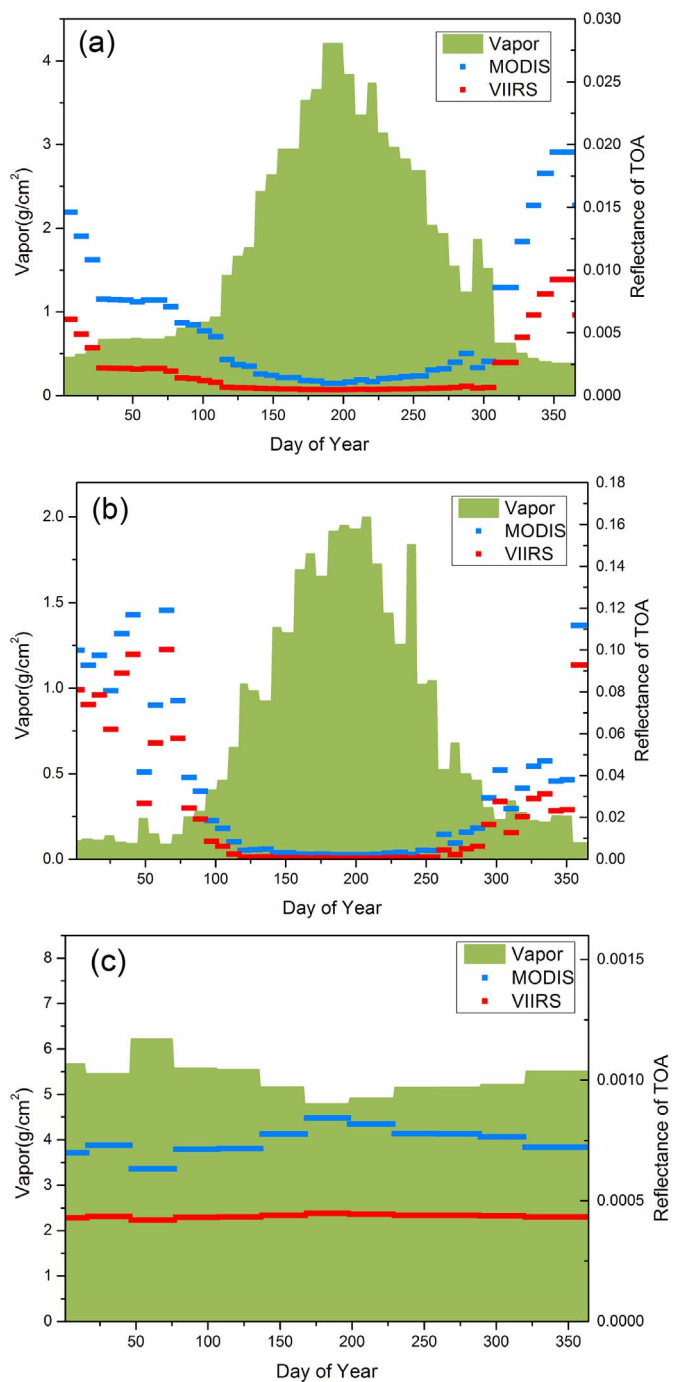


Fig. 8. Simulated annual variations in clear-sky reflectance for the VIIRS and the MODIS cirrus cloud channels using observed water vapor as inputs over (a) a mid-latitude region, (b) a sub-polar region, and (c) a tropical region.

the reflectance of the VIIRS M9 and the MODIS band 26. The VIIRS M9 decreases the TOA reflectance by about 41.5% compared with the MODIS band 26.

4. Comparative analysis with CALIOP data

Section 3 gave detailed simulation analysis for the VIIRS M9 channel and the MODIS channel 26, in this section we compared the MODIS channel 26 and the VIIRS M9 channel measurements for non-cirrus cloud, cirrus cloud and clear-sky cases as identified by CALIOP.

4.1. Data processing

CALIP, as a Lidar, has a congenital advantage in providing the profile information of the atmospheric, and is often employed by researchers to validate the accuracy of the algorithms used to retrieve the cloud parameter (Holz et al., 2008; Hutchison et al., 2014). In order to use CALIP VFM data to evaluate the MODIS channel 26 and the VIIRS M9 channel, the first step is to get the matching datasets of CALIP, MODIS and VIIRS for the same geographical position with similar imaging time. In the study, the method proposed by Nagle and Holz (2009) was used to obtain such match-ups. Due to the fact that CALIP has high sensitivity to cloud tops and optically thin cirrus clouds (Winker et al., 2007), or multi-layer clouds exist, a new rule to redefine the cirrus cloud pixel was that the pixel of this VFM data would be recognized as a cirrus cloud, only when the top-layer cloud information of the VFM data is cirrus cloud and the continuous distribution of cirrus cloud layers is no less than 5 (Xia et al., 2015). This rule was also used to define the non-cirrus cloud pixel in the study. Then, the match-up pixels were divided into three types: cirrus cloud pixels, non-cirrus cloud pixels, perfect clear-sky pixels. Perfect clear-sky pixel means perfect clear in both three sensors, and the non-cirrus cloud pixel is covered by non-cirrus cloud in both three sensors. The cirrus cloud pixel is just based on the result observed by CALIP. The MODIS and VIIRS cloud mask products were used to identify the clear or cloudy status of the sky for MODIS and VIIRS observation respectively (Frey et al., 2008; Hutchison et al., 2012).

When validating the performance of the VIIRS cloud mask product by CALIP, Hutchison [Hutchison et al., 2014] limited the imaging interval between VIIRS and CALIP within 20 min. In this study, we also adopted this rule that the imaging interval between the MODIS, VIIRS and CALIP should be less than 20 min. In most cases, the maximum imaging interval of 20 min is acceptable to evaluate the performance difference between the VIIRS M9 and the MODIS band 26 over non-cirrus cloud, because most of non-cirrus clouds usually move slower than the cirrus cloud. However, 20 min is too large to evaluate performance difference between VIIRS and MODIS cirrus channel over cirrus cloud, for some of the cirrus clouds located at upper troposphere where wind speed is strong over this region. The strong wind means cirrus clouds can move dozens pixels within 20 min, as a result, the object at the same geolocation observed by CALIP, MODIS and VIIRS may be totally different. Hence, additional rules should be applied to filter the obtained data for cirrus cloud pixels.

According to the study by Garnier et al. (2017), when assessing the performance of the CALIPSO Imaging Infrared Radiometer (IIR) through MODIS data, the brightness temperature difference of 11 μm channels between MODIS and IIR was limited to ± 2.1 K to eliminate match-up pixels with different cloud contamination. In this study, this criterion was employed for the cirrus cloud match-up pixels, the brightness temperatures of 11 μm for the same pixel observed by the two sensors should have a difference less than 2.1 K. Besides, according to the simulation results, if the value of the match-up pixel calculated by Eq. (2) is less than -1.5 or greater than 0.5 , then this match-up pixel will be eliminated.

4.2. Results

CALIP, VIIRS and MODIS data from January to September of 2014 over the Tibetan Plateau, the U.S., the equator region, the sub-Arctic region and Africa were downloaded from the Atmospheric Science Data Center (ASDC) at the NASA Langley Research Center and the GSFC Level 1 and atmosphere Archive and Distribution system, to evaluate the cirrus channel performance difference between the VIIRS and the MODIS cirrus cloud channels. These regions are representative areas for evaluating the actual performance between the MODIS band 26 and the VIIRS M9 over different surface types, elevations, vapor content. More information about the regions is listed in Table 5.

Table 5
Information for the regions used in the study.

Region	Geo-location (°)	Main surface type	Mean Elevation (m)
Tibetan Plateau	27–35 N, 83–95 E	Bare land	4000
U.S.	27–33 N, 89–92 W	Grassland	50.0
Equator	0 E–10 N, 100–110 E	Sea water	0.0
Subarctic	57–62 N, 108–112 E	Forest	450
Africa	20–29 N, 19–30 W	Desert	300

As the simulation analysis showed in Section 3.3, the TOA reflectance difference between the VIIRS M9 and the MODIS band 26 depended on cloud type and was substantially influenced by cloud altitude. Hence, this study used the x-axis to represent cloud-top altitude, which was obtained from the CALIP VFM data, and the y-axis to represent the reflectance difference between the MODIS band 26 and the VIIRS M9, as shown in Fig. 9.

As shown in Fig. 9, for a region with ample water vapor content, e.g., the equator region, the high water vapor content masks almost all background reflectance from the surface or cloud with low cloud-top altitude. As a result, the reflectance difference between the VIIRS M9 and the MODIS band 26 is small when the cloud-top altitude is less than 4 km or the sky is perfectly clear, as the blue or orange points shown in Fig. 9(a). For a region with low vapor content, e.g., the Tibetan Plateau region shown in Fig. 9(d), the situation is opposite. High surface elevation and low vapor content in the Tibetan Plateau region, shown as the blue and orange points in Fig. 9(d), cause substantial background reflectance for both clear-sky and non-cirrus cloud. The reflectance difference between the VIIRS M9 and the MODIS band 26 is greater than in other regions. In addition, for the non-cirrus cloud pixels shown in the mid-latitude region (U.S.), Africa desert region and the sub-Arctic region, the reflectance differences between the VIIRS M9 and the MODIS band 26 demonstrate a similar trend with those shown in the equator region. In general, almost all of the non-cirrus cloud and clear-sky pixels reflectance differences shown in Fig. 9 are greater than 0, which is in agreement with the simulation results for non-cirrus clouds and clear-sky showed in Section 3. This means the VIIRS M9 is more efficient to decrease the clear-sky background reflectance than the MODIS band 26.

For cirrus cloud in the equator region (Fig. 9(a)), most of the cirrus cloud reflectance differences (red points) are non-negative. It indicates the MODIS band 26 displays greater reflectance than the VIIRS M9 for cirrus cloud, which is inconsistent with the simulation results shown in Section 3.3 Fig. 6 (a) and (b). However, for other regions, such as the U.S., Africa, and the sub-Arctic regions, the reflectance variations with the cloud-top altitude are coincidental with the simulation results shown in Section 3.3 Fig. 6(b). The reflectance differences (red points) in Fig. 9(b), (c) and (e) show that as the cloud-top altitude increasing, the reflectance differences between the VIIRS M9 and the MODIS band 26 decline. Especially, when the cloud-top altitude is higher, e.g., 14 km, the VIIRS M9 represents similar and even slightly larger reflectance than the MODIS band 26.

The inconsistent results for the cirrus cloud reflectance difference between the equator and other regions are primarily due to the different troposphere depths which lead to different amounts of water vapor around the cirrus cloud layer and different atmosphere profile. In the equator region, the average depths of the troposphere are 20 km, which is higher than in other regions, e.g., 17 km in the mid-latitude region and 7 km in the polar region. The higher depth of the troposphere provides more vapor content between the cirrus cloud and sensor in the equator than other regions. When the cirrus cloud altitudes over the equator and other regions are equal, the large amount of vapor content in the equator results in a smaller cirrus cloud reflectance for the VIIRS M9. However, as the cirrus cloud-top altitude increases to 18 km, as shown in Fig. 9(a), the amount of water vapor between the

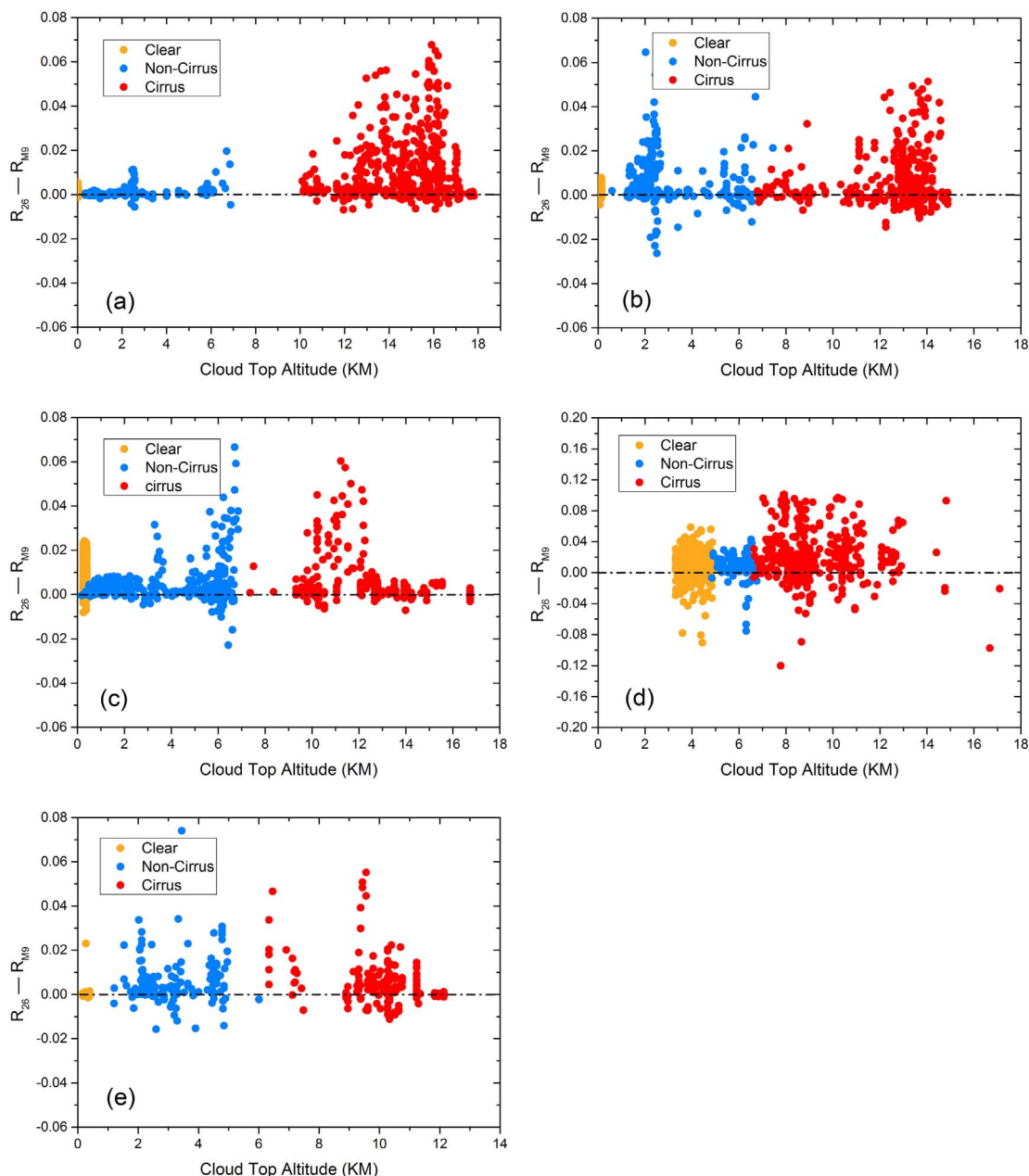


Fig. 9. Actual reflectance difference of the VIIRS and the MODIS cirrus cloud band in different regions: (a) tropical, (b) mid-latitude (U.S.), (c) Africa (desert), (d) high-altitude (Tibetan Plateau) and (e) sub-Arctic. (For interpretation of the references to color in this figure, the reader is referred to the web version of this article.)

cirrus cloud top and sensors can almost be ignored, and the reflectance values between the VIIRS M9 and the MODIS band 26 are similar.

The mean reflectance of the MODIS and VIIRS cirrus channels, as well as variation percentages of reflectance calculated by Eq. (2) in the Tibetan Plateau, the equator, the sub-Arctic, Africa and the U.S. regions are shown in Table 6. The mean variation percentage of reflectance for clear sky is 35.96%, close to the result shown in Section 3.4, and the mean variation percentage of reflectance for non-cirrus cloud is 29.86%. Due to the large vapor content between the cirrus cloud and sensors, as it mentioned above, a larger variation percentage of reflectance for cirrus cloud was presented in the equator region (28.83%), than other regions. Considering this point, in the equator region, the narrower band design of the VIIRS M9 band may not perform as better as it shown in other regions.

In order to make the result of the study be used as a reference to design a precise cirrus test method, the detailed reflectance over each region is listed in Table 6. As shown in Table 6, in the equator region,

due to the ample vapor, the reflectances of non-cirrus cloud and clear-sky for both the MODIS band 26 and VIIRS M9 are smaller than other regions. In general, the VIIRS M9 has lower clear-sky reflectance of 0.0095 than MODIS of 0.0133. This difference indicates the cirrus cloud detection threshold of VIIRS can be set smaller than MODIS, so more thin cirrus can be recognized by the VIIRS. Besides, as can be seen in Table 6, both the reflectances of non-cirrus cloud and clear-sky differ in the U.S., Africa, the equator, therefore, region-orientated algorithms should be designed for the cirrus cloud detection.

In addition, as shown in Table 6, the reflectance over the Tibetan Plateau region for both cirrus cloud, non-cirrus cloud and clear-sky are greater than other regions, e.g. the clear-sky reflectance of 0.092 and 0.081 for the MODIS and VIIRS cirrus channels in the Tibetan Plateau. This difference is due to the extremely low vapor content causing substantial background reflectance, which passes through cirrus clouds and is detected by the sensor. In fact, due to the substantial background reflectance, the current MODIS and VIIRS 1.38 μm cirrus cloud

Table 6

The statistical information of reflectance in the Tibetan Plateau, the equator, the sub-Arctic, Africa and the U.S. MN stands for pixel number of match-up; MR indicates mean reflectance for the MODIS and VIIRS 1.38 μm channel respectively; PV represents variation percentage of reflectance calculated by Eq. (2) with unit %.

Region	Cirrus cloud			Non-cirrus cloud			Clear sky		
	MN	MR	PV	MN	MR	PV	MN	MR	PV
Tibetan Plateau	827	0.1321/0.108	13.54	618	0.080/0.071	14.48	1624	0.0920/0.0810	12.58
Equator	517	0.089/0.075	28.83	726	0.007/0.005	20.48	867	0.0010/0.0008	23.34
Subarctic	608	0.033/0.027	12.01	546	0.014/0.009	34.20	649	0.0020/0.0014	28.62
Africa	512	0.037/0.029	5.03	1546	0.015/0.006	24.52	7950	0.0061/0.0028	41.79
U.S.	876	0.049/0.039	4.72	727	0.022/0.017	27.2	1374	0.0089/0.0062	28.77
Mean	3340	0.084/0.067	12.63	4163	0.020/0.015	29.86	12,464	0.0133/0.0095	35.96

algorithm usually fails to perform over this region in winter (Frey et al., 2008; Hutchison et al., 2012). Hence, the feature that the temperature of the cirrus cloud is lower than the surface (Xia et al., 2015) or other composite of other bands might be used to improve the performance of cirrus cloud test.

5. Conclusions

In this study, the Visible Infrared Imaging Radiometer (VIIRS) and the Moderate Resolution Imaging Spectroradiometer (MODIS) cirrus cloud channels were compared using simulated and actual observed data. The comparison analyses using simulated and actual MODIS, VIIRS and Cloud-Aerosol Lidar with Orthogonal Polarization (CALIOP) data show that the improved VIIRS M9 channel, which has a narrower bandwidth and a removed out-of-band response effect, performs better than the MODIS band 26. The simulation results indicate the VIIRS M9 can reduce clear-sky background reflectance by approximately 66.7%, 52.6% and 41.5% compared with the MODIS band 26 in the surface of sandstone over mid-latitude, sub-Arctic and tropical regions. The analyses based on actual observation data show that the VIIRS M9 can reduce non-cirrus cloud reflectance by 29.86% and reduce clear-sky reflectance by 35.96% compared with the MODIS band 26.

Although MODIS and VIIRS have substantial capabilities for detecting cirrus clouds, according to the analyses in this study, we still face challenges when using the 1.38 μm band to gain more accurate cirrus information. First, different regions have different atmospheric conditions, including water vapor content and surface characteristics that create different background reflectance, so a constant threshold for the entire test is inaccurate. Second, for some regions with low vapor content, the background reflectance caused by low vapor is greater than the cirrus cloud reflectance, so the current test will fail to perform. Third, non-cirrus clouds with high altitude, especially stratus clouds, will be misclassified as cirrus clouds when a relatively low threshold is used. On the whole, further studies needs to be done regarding the 1.38 μm cirrus test to provide more accurate cirrus cloud identification.

Acknowledgments

We would thank Dr. F. W. Nagle in University of Wisconsin-Madison for providing procedure to collocate MODIS, VIIRS and CALIOP data, Dr. Aisheng Wu in Science Systems and Applications, Inc. for providing help about MODIS data, the National Oceanic and Atmospheric Administration, the Goddard Space Flight Center for providing VIIRS, MODIS, CALIOP data.

This work was supported by Natural Science Foundation of China (No. 41571427, 31601228), Natural Key Project of China (No. 2016YFC0500203, 2016YFD0200700), Innovative group guide project (Grant No. Y2017JC33) and Open Fund of State Key Laboratory of Remote Sensing Science (Grant No. OFSLRSS201708).

The authors thank three anonymous reviewers for their constructive and helpful comments.

References

- Ackerman, S.A., Strabala, K.I., Paul, M.W., Frey, R.A., Moeller, C.C., Gumley, L.E., 1999. Discriminating clear sky from clouds with modis. *J. Geophys. Res. Atmos.* 103 (D24), 32141–32157.
- Baker, N., 2014. Joint Polar Satellite System (JPSS) VIIRS Cloud Mask (VCM) Algorithm Theoretical Basis Document (ATBD), Rev D (Accessed June 4, 2014. Available online at). http://npp.gsfc.nasa.gov/sciencedocuments/2014-07/474-00033_ATBD-VIIRS-Cloud-Mask_D.pdf.
- Baldrige, A.M., Hook, S.J., Grove, C.I., Rivera, G., 2009. The ASTER spectral library version 2.0. *Remote Sens. Environ.* 113 (4), 711–715.
- Barsi, J.A., Lee, K., Kvaran, G., Markham, B.L., Pedelty, J.A., 2014. The spectral response of the Landsat-8 operational land imager. *Remote Sens.* 6 (10), 10232–10251.
- Baum, B.A., Yang, P., Heymsfield, A.J., Bansemir, A., Cole, B.H., Merrelli, A., ... Wang, C., 2014. Ice cloud single-scattering property models with the full phase matrix at wavelengths from 0.2 to 100 μm . *J. Quant. Spectrosc. Radiat. Transf.* 146, 123–139.
- Berk, A., Anderson, G.P., Acharya, P.K., Bernstein, L.S., Muratov, L., Lee, J., et al., 2005. Modtran 5: a reformulated atmospheric band model with auxiliary species and practical multiple scattering options: update. In: *Proceedings of SPIE - The International Society for Optical Engineering*. 5806. pp. 662–667.
- Buras, R., Dowling, T., Emde, C., 2011. New secondary-scattering correction in DISORT with increased efficiency for forward scattering. *J. Quant. Spectrosc. Radiat. Transf.* 112 (12), 2028–2034.
- Cao, C., Xiong, J., Blonski, S., Liu, Q., Upreti, S., Shao, X., ... Weng, F., 2013. Suomi NPP VIIRS sensor data record verification, validation, and long-term performance monitoring. *J. Geophys. Res. Atmos.* 118 (20).
- Chan, M.A., Comiso, J.C., 2011. Cloud features detected by MODIS but not by CloudSat and CALIOP. *Geophys. Res. Lett.* 38 (24).
- Drusch, M., Del Bello, U., Carlier, S., Colin, O., Fernandez, V., Gascon, F., ... Meygret, A., 2012. Sentinel-2: ESA's optical high-resolution mission for GMES operational services. *Remote Sens. Environ.* 120, 25–36.
- Emde, C., Buras-Schnell, R., Kylling, A., Mayer, B., Gasteiger, J., Hamann, U., ... Bugliaro, L., 2016. The libRadtran software package for radiative transfer calculations (version 2.0.1). *Geosci. Model Dev.* 9 (5), 1647–1672.
- Frey, R.A., Ackerman, S.A., Liu, Y., Strabala, K.I., Zhang, H., Key, J.R., Wang, X., 2008. Cloud detection with MODIS. Part I: improvements in the MODIS cloud mask for collection 5. *J. Atmos. Ocean. Technol.* 25 (7), 1057–1072.
- Fu, Q., 1996. An accurate parameterization of the solar radiative properties of cirrus clouds for climate models. *J. Clim.* 9 (9), 2058–2082.
- Gao, B.C., Kaufman, Y.J., 1995. Selection of the 1.375- μm MODIS channel for remote sensing of cirrus clouds and stratospheric aerosols from space. *J. Atmos. Sci.* 52 (23), 4231–4237.
- Gao, B.C., Goetz, A.F., Wiscombe, W.J., 1993. Cirrus cloud detection from airborne imaging spectrometer data using the 1.38 μm water vapor band. *Geophys. Res. Lett.* 20 (4), 301–304.
- Gao, B.C., Kaufman, Y.J., Tanre, D., Li, R.R., 2002. Distinguishing tropospheric aerosols from thin cirrus clouds for improved aerosol retrievals using the ratio of 1.38- μm and 1.24- μm channels. *Geophys. Res. Lett.* 29 (18).
- Garnier, A., Scott, N.A., Pelon, J., Armante, R., Crépeau, L., Six, B., Pascal, N., 2017. Long-term assessment of the CALIPSO Imaging Infrared Radiometer (IIR) calibration and stability through simulated and observed comparisons with MODIS/Aqua and SEVIRI/Meteosat. *Atmos. Meas. Tech.* 10 (4), 1403.
- Gasteiger, J., Emde, C., Mayer, B., Buras, R., Buehler, S.A., Lemke, O., 2014. Representative wavelengths absorption parameterization applied to satellite channels and spectral bands. *J. Quant. Spectrosc. Radiat. Transf.* 148, 99–115.
- Hirakata, Maki, Okamoto, Hajime, Hagiwara, Yuichiro, Hayasaka, Tadahiro, Oki, Riko, 2014. Comparison of global and seasonal characteristics of cloud phase and horizontal ice plates derived from CALIPSO with MODIS and ECMWF. *J. Atmos. Ocean. Technol.* 31, 2114–2130. <http://dx.doi.org/10.1175/JTECH-D-13-00245.1>.
- Holz, R.E., Ackerman, S.A., Nagle, F.W., Frey, R., Dutcher, S., Kuehn, R.E., ... Baum, B., 2008. Global Moderate Resolution Imaging Spectroradiometer (MODIS) cloud detection and height evaluation using CALIOP. *J. Geophys. Res. Atmos.* 113 (D8).
- Hu, Y.X., Stannnes, K., 1993. An accurate parameterization of the radiative properties of water clouds suitable for use in climate models. *J. Clim.* 6 (4), 728–742.
- Hubanks, Platnick, King, Ridgway, 2015. Modis Atmosphere L3 Gridded Product Algorithm Theoretical Basis Document. (ATBD, Reference Number: ATBD-MOD-30).
- Hunt, W.H., Winker, D.M., Vaughan, M.A., Powell, K.A., Lucker, P.L., Weimer, C., 2009. Calipso lidar description and performance assessment. *J. Atmos. Ocean. Technol.* 26

- (7), 1214–1228.
- Hutchison, K.D., Iisager, B.D., Hauss, B., 2012. The use of global synthetic data for pre-launch tuning of the VIIRS cloud mask algorithm. *Int. J. Remote Sens.* 33 (5), 1400–1423.
- Hutchison, K.D., Heidinger, A.K., Kopp, T.J., Iisager, B.D., Frey, R.A., 2014. Comparisons between VIIRS cloud mask performance results from manually generated cloud masks of VIIRS imagery and CALIOP-VIIRS match-ups. *Int. J. Remote Sens.* 35 (13), 4905–4922.
- Justice, C.O., Vermote, E., Townshend, J.R., Defries, R., Roy, D.P., Hall, D.K., ... Lucht, W., 1998. The Moderate Resolution Imaging Spectroradiometer (MODIS): land remote sensing for global change research. *IEEE Trans. Geosci. Remote Sens.* 36 (4), 1228–1249.
- Justice, C.O., Townshend, J.R.G., Vermote, E.F., Masuoka, E., Wolfe, R.E., Saleous, N., et al., 2002. An overview of modis land data processing and product status. *Remote Sens. Environ.* 83 (1–2), 3–15.
- Kaufman, Y.J., Gao, B.C., 1992. Remote sensing of water vapor in the near IR from EOS/MODIS. *IEEE Trans. Geosci. Remote Sens.* 30 (5), 871–884.
- Kazantzidis, A., Eleftheratos, K., Zerefos, C.S., 2011. Effects of cirrus cloudiness on sun irradiance in four spectral bands. *Atmos. Res.* 102 (4), 452–459.
- Key, J.R., Yang, P., Baum, B.A., Nasiri, S.L., 2002. Parameterization of shortwave ice cloud optical properties for various particle habits. *J. Geophys. Res.: Atmos.* 107 (D13).
- Kovalsky, Valeriy, Roy, D., 2015. A one year Landsat 8 conterminous United States study of cirrus and non-cirrus clouds. *Remote Sens.* 7 (1), 564–578.
- Liou, K.N., 1973. Transfer of solar irradiance through cirrus cloud layers. *J. Geophys. Res.* 78 (9), 1409–1418.
- Liou, K.N., 2002. *An Introduction to Atmospheric Radiation*. vol. 84 Academic Press.
- Mayer, B., Kylling, A., 2005. Technical note: the libRadtran software package for radiative transfer calculations – description and examples of use. *Atmos. Chem. Phys.* 5, 1855–1877.
- Nagle, F.W., Holz, R.E., 2009. Computationally efficient methods of collocating satellite, aircraft, and ground observations. *J. Atmos. Ocean. Technol.* 26 (8), 1585–1595.
- Roskovensky, J.K., Liou, K.N., 2003. Detection of thin cirrus from 1.38 μm /0.65 μm reflectance ratio combined with 8.6–11 μm brightness temperature difference. *Geophys. Res. Lett.* 30 (19).
- Roy, D.P., Wulder, M.A., Loveland, T.R., Woodcock, C.E., Allen, R.G., Anderson, M.C., ... Scambos, T.A., 2014. Landsat-8: science and product vision for terrestrial global change research. *Remote Sens. Environ.* 145, 154–172.
- Stamnes, K., Tsay, S.C., Wiscombe, W., Jayaweera, K., 1988. Numerically stable algorithm for discrete-ordinate-method radiative transfer in multiple scattering and emitting layered media. *Appl. Opt.* 27 (12), 2502–2509.
- Sun, W., Lin, B., Hu, Y., Lukashin, C., Kato, S., Liu, Z., 2011. On the consistency of CERES longwave flux and AIRS temperature and humidity profiles. *J. Geophys. Res. Atmos.* 116 (D17).
- Toller, G.N., Isaacman, A., Leader, M.T., Salomonson, V., 2003. *MODIS Level 1b Product User's Guide*. (Signature).
- Upreti, S., Cao, C., Xiong, X., Blonski, S., Wu, A., Shao, X., 2013. Radiometric inter-comparison between Suomi-NPP VIIRS and Aqua MODIS reflective solar bands using simultaneous nadir overpass in the low latitudes. *J. Atmos. Ocean. Technol.* 30 (12), 2720–2736.
- Wendisch, M., Yang, P., 2012. *Theory of Atmospheric Radiative Transfer*. John Wiley & Sons.
- Winker, D.M., Pelon, J., McCormick, M.P., Hunt, W.H., McGill, M.J., 2007. Initial performance assessment of CALIOP. *Geophys. Res. Lett.* 34, L19803.
- Xia, L., Mao, K., Ma, Y., Zhao, F., Jiang, L., Shen, X., Qin, Z., 2014. An algorithm for retrieving land surface temperatures using VIIRS data in combination with multi-sensors. *Sensors* 14 (11), 21385–21408.
- Xia, L., Zhao, F., Ma, Y., Sun, Z.W., Shen, X.Y., Mao, K.B., 2015. An improved algorithm for the detection of cirrus clouds in the Tibetan Plateau using VIIRS and MODIS data. *J. Atmos. Ocean. Technol.* 32 (11), 2125–2129.
- Xiong, X., Chiang, K.F., Adimi, F., Li, W., Yatagai, H., Barnes, W.L., 2004. MODIS correction algorithm for out-of-band response in the short-wave IR bands. In: *Remote Sensing*. International Society for Optics and Photonics, pp. 605–613.
- Xiong, X., Butler, J., Chiang, K., Efremova, B., Fulbright, J., Lei, N., ... Wu, A., 2014. VIIRS on-orbit calibration methodology and performance. *J. Geophys. Res. Atmos.* 119 (9), 5065–5078.
- Xu, Lisheng, 2002. Light scattering characteristics of small ice circular cylinders in visible, 1.38 μm , and some infrared wavelengths. *Opt. Eng.* 41 (9), 2252.
- Yang, P., Gao, B.C., Baum, B.A., Wiscombe, W.J., Hu, Y.X., Nasiri, S.L., ... Miloshevich, L.M., 2001. Sensitivity of cirrus bidirectional reflectance to vertical inhomogeneity of ice crystal habits and size distributions for two Moderate-Resolution Imaging Spectroradiometer (MODIS) bands. *J. Geophys. Res. Atmos.* 106 (D15), 17267–17291.
- Yang, P., Bi, L., Baum, B.A., Liou, K.N., Kattawar, G.W., Mishchenko, M.I., Cole, B., 2013. Spectrally consistent scattering, absorption, and polarization properties of atmospheric ice crystals at wavelengths from 0.2 to 100 μm . *J. Atmos. Sci.* 70 (1), 330–347.